Journal of the European Ceramic Society **14** (1994) 97–109

Reaction Bonding of Aluminum Oxide (RBAO) Composites: Processing, Reaction Mechanisms and Properties

Nils Claussen, Suxing Wu & Dietmar Holz

Technische Universität Hamburg-Harburg, Advanced Ceramics Group, 21071 Hamburg, Germany

Dedicated to Professor Hansjörg Sinn on the occasion of his 65th birthday

(Received 4 November 1993; revised version received 22 November 1993; accepted 28 January 1994)

Abstract

As an alternative to conventional Al_2O_3 manufacturing, a novel technique, reaction bonding of aluminum oxide (RBAO), has been successfully developed. Although the technique is in its infancy, it has already demonstrated interesting characteristics, such as high green strength without organic additives, low-to-zero shrinkage tailorability, superior mechanical properties, superplastic transformability and broad microstructural versatility. One of the important technical potentials is to use RBAO as a matrix for large-scale second-phase particles, e.g. platelets and fibers, without causing the harmful residual stresses normally encountered with shrinking matrix materials.

Das Reaktionsbinden von Aluminiumoxid (RBAO) ist ein neuartiges Verfahren zur Herstellung von schwindungsarmen Al_2O_3-Keramiken. RBAO-Werkstoffe zeichnen sich im Gegensatz zu konventionell hergestelltem Al_2O_3 durch hohe Grünfestigkeit ohne Zusatz von organischen Bindern, ein Near-Net-Shape Potential, deutlich verbesserte mechanische Eigenschaften, superplastische Umformbarkeit und die Möglichkeit der Modifizierung der Mikrostruktur in einem weiten Bereich aus. Besonders hervorzuheben ist das technische Potential von RBAO-Keramiken als Matrixwerkstoff für faser- oder plättchenverstärkte Verbundwerkstoffe, da die normalerweise auftretenden inneren Spannungen um Verstärkungsteilchen herum durch die reduzierte Sinterschrumpfung vermindert werden.

On a réussi à développer une nouvelle technique de fabrication d'Al_2O_3, la liaison réactionnelle de l'oxyde d'aluminium (RBAO). Bien que les développements de cette technique soient à leurs débuts, les matériaux obtenus présentent déjà des caractéristiques intéressantes, telles qu'une bonne résistance du produit brut sans addition de produits organiques, la possibilité de réduire le rétrécissement jusqu'à des valeurs proches de zéro, une amélioration nette des propriétés mécaniques, des qualités superplastiques et un large choix de microstructures. Une des applications importantes de la RBAO serait la fabrication de matrices contenant des particules de seconde phase de grande taille (plaquettes, fibres), sans le désavantage des contraintes résiduelles usuellement provoquées par le rétrécissement de la matrice.

1 Introduction

Reaction forming of ceramics exhibits various advantages when compared with conventional manufacturing. Low raw materials costs, near-net-shape tailorability, and glass-phase-free grain boundaries, are most attractive attributes for many technical and high performance applications. Especially the low-to-zero shrinkage capability makes most reaction-forming techniques suitable for the fabrication of composites. Research and development activities have mainly emphasized non-oxide ceramics, such as RBSN, RBSC and CVD-SiC. Oxidation reactions have been widely studied, although not usually for the sake of producing ceramics. Only a few years ago, the directed oxidation of molten metals (DMO) was introduced.[1–4] In this technique Al/Al_2O_3 composites are produced by oxidizing molten Al alloys.

Thereafter, another oxidation forming technique, reaction bonding of aluminum oxide (RBAO), was developed at the Technische Universität Hamburg–Harburg.[5–9] In this technique, attrition-

Journal of the European Ceramic Society 0955-2219/94/$7.00

milled Al/Al_2O_3 powder compacts are heat treated in air such that Al oxidizes to small 'new' Al_2O_3 crystallites, which sinter and thereby bond together the originally added Al_2O_3 or other ceramic particles.

The oxidation of Al particles thus represents the key for a new technology leading to novel Al_2O_3-based composites. The main features of these composites are reduced shrinkage and high strength. The low shrinkage results from partial compensation of the sintering shrinkage by an expansion associated with the oxidation. The high strength is due to the fine grain size (<1 μm) which develops during the reaction-bonding process. This is also why RBAO ceramics are superplastically transformable. The low-to-zero shrinkage tailorability especially of mullite RBAO represents an ideal matrix for the stress-free incorporation of large-scale (>50 μm) second phases (e.g. sapphire fibers). The potential for versatile microstructure development and novel composites attracts increased interest.

The present paper summarizes the present state-of-art by describing the principles, reaction mechanisms, modifications, microstructures and mechanical properties of RBAO ceramics.

2 Principles

The RBAO process starts from Al metal (usually 30 to 60 vol.%) and Al_2O_3 powder mixtures. To improve microstructure and mechanical properties, 5–20 vol.% ZrO_2 is usually added. The mixtures are intensively mixed in an attrition mill, normally with ZrO_2 milling media (e.g. 3Y-TZP), such that the Al (~20–200 μm) is reduced to small particles (<1 μm) with Al_2O_3 and ZrO_2 dispersions consisting of powders in the tens of nanometer size range.[8,9] In addition to the admixed components, Al_2O_3 and ZrO_2 dispersions also result from Al oxidation products caused by the milling process and the wear debris of the milling balls, respectively. After milling, the powder mixtures are passivated such as to allow safe handling in air.

Any green compaction technique can be applied to form the required shapes. As shown schematically in Fig. 1, Al particles are plastically deformed, which results in strong Al/Al contacts bridging the Al_2O_3 particles. Therefore, green density is high and green strength attains values more than an order of magnitude higher (20–50 MPa) than those of conventional ceramic green bodies.[6,9] For this reason, green machining can readily be applied to the RBAO powder compacts.

On heating the compacts in oxidizing atmosphere (usually air), at temperatures >350°C (reaction range), Al oxidizes to Al_2O_3. Regardless of the complex nature of the oxidation reaction, the final product is α-Al_2O_3 giving a net volume expansion of 28%. In the sintering range at >1200°C, the body shrinks, compensating for the expansion. However, in the 'pure' RBAO system in which only Al and Al_2O_3 are present, up to 15% linear shrinkage still remains when the final density exceeds 95% TD. Hence the expansion due to the oxidation of Al is not sufficient. In order to further reduce the shrinkage and even to achieve net-shape forming, the RBAO process can be modified in various ways by incorporating other metal or ceramic additives that exhibit a larger volume expansion on oxidation. For instance, Zr is associated with a volume expansion on oxida-

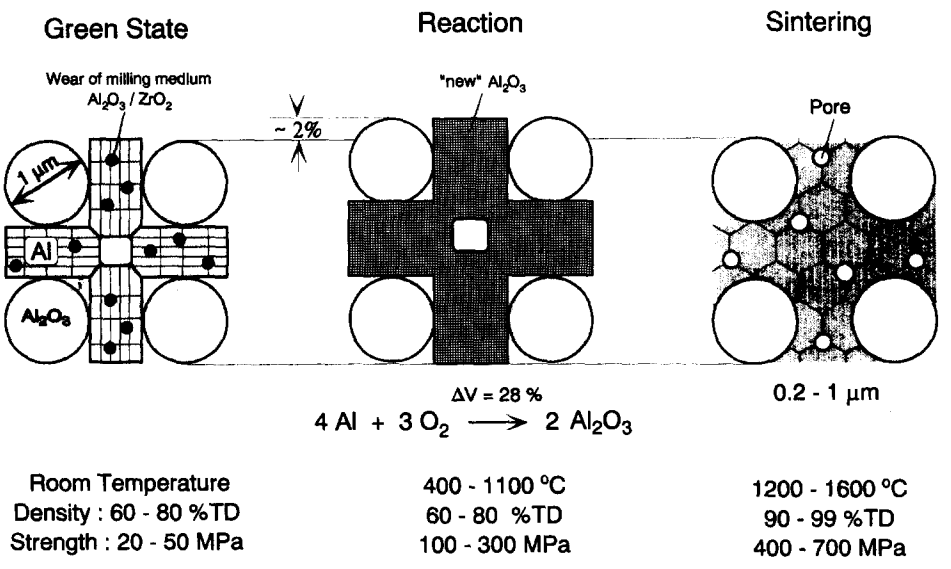

Fig. 1. Schematic diagram of the RBAO process. In the green state, 'old' Al_2O_3 particles are bridged by Al particles containing oxide dispersions from mechanical alloying. In the reaction stage, associated with an expansion, Al transforms to nano-sized Al_2O_3 particles which sinter at temperatures >1200°C.

tion of 49%, Ti 76%, Cr 102%, Nb 174% and, when forming mullite from the addition of SiC via SiO_2, the change is 132%. A general equation predicting the total dimensional change, S, after a complete reaction-bonding cycle is given by

$$S = \left(\frac{1 + \sum \nu_i V_i}{1 + \alpha f V_{Al}} \cdot \frac{\rho_0}{\rho}\right)^{1/3} - 1 \qquad (1)$$

where ν_i is the volume expansion associated with the respective oxidation (e.g., $\nu_{Al} = 0{\cdot}28$), V_i is the volume fraction of metal or ceramic phases added to the original powder mixture, $\alpha(\sim 0{\cdot}6)$ is the volume expansion associated with the oxidation of Al to amorphous Al_2O_3 during milling, f is the Al fraction oxidized during milling, and ρ_0 and ρ are the green and final densities, respectively.

3 The RBAO Process

3.1 Characterization

The RBAO process has been intensively characterized by dilatometry and thermogravimetry.[6–9] Unlike the DMO process, the oxidation reaction of Al takes place already at rather low temperatures (>350°C) and does not depend on any additives. Before the oxidation reaction taking place, the heating of the RBAO powder compact is associated with a weight loss due to evaporation of fugitive species. In addition to the organic gas of milling fluid used, H_2O and H_2 are responsible for the weight loss. Wet milling and handling dried powder in air is accompanied by water uptake and hydrolysis in the surface region of Al particles. The desorption of the water and the decomposition of the hydrolysis products, boehmite and diaspore, release the gases. It has been commonly observed that the oxidation exhibits a maximum reaction rate at ~520°C. At temperatures between ~520 and 660°C the reaction rate is reduced and only limited Al is oxidized (<5%). Under normal experimental conditions with Al particle sizes <1 μm, ~60% Al oxidizes by way of the solid/gas reaction. The melting of Al (660°C) is only associated with limited densification. Extended particle rearrangement such as is typically true for liquid-phase sintering is not observed. The oxide skin on the Al particles developed during milling and oxidation prevents much redistribution of the molten Al. Above the melting point of Al, although the reaction system exhibits a large weight gain, the dimensional change remains almost constant indicating that further reaction proceeds with the filling of voids by the oxide products.

The reaction products at <450°C are mainly amorphous Al_2O_3, with only traces of crystalline γ-Al_2O_3 being identified by XRD, but at >450°C significant γ-Al_2O_3 begins to appear.[8] Between ~900 and ~1200°C, some shrinkage occurs. Rather than sintering, this is attributed to the γ- to α-Al_2O_3 phase transformation associated with a 7·6% volume decrease. γ-Al_2O_3 is nearly fully transformed to α-Al_2O_3 at ~1150°C. However, when ZrO_2 is present, the transformation temperature is raised by ~100°C, which is consistent with the literature[10] reporting that ZrO_2 additions strongly retard the γ- to α-Al_2O_3 phase transformation. At slow heating rates (~1°C/min), the oxidation reaction of Al is usually completed at temperatures <1000°C; i.e. molten regions within the Al particles have been fully replaced by small 'new' Al_2O_3 crystals. Due to the extremely fine particle size, sintering starts already at temperatures >1200°C.

In the sintering range T > 1200°C, 'old' Al_2O_3 particles are bonded by the 'new' crystals and grain growth takes place. In the final fully reaction-bonded body, 'new' and 'old' particles can no longer be distinguished, in contrast to the observations in partially reacted compacts.

3.2 Mechanisms

The reaction-bonding mechanisms for the RBAO process by which complete oxidation is achieved have been studied.[8] At temperatures <450°C, the amorphous thin passivating skin, coating the Al particles during milling grows by Al^{3+} ions diffusing outward through the oxide layer and reacting with oxygen.[11] However, this mechanism contributes only little (<5%) to the total oxidation. At temperatures >450°C, Al oxidizes directly to crystalline γ-Al_2O_3, and the preexisting amorphous phase also crystallizes to γ-Al_2O_3. Oxygen diffuses along grain boundaries in the oxide skin which, due to its incoherent nature and the ultrafine grain size of the 'new' Al_2O_3 crystals, offers an effective transport path. Because of the 39% volume expansion associated with the Al → γ-Al_2O_3 oxidation reaction, microcracks are formed in the oxide skin, providing extra oxygen access. The volume expansion caused by the reaction, the thermal mismatch due to the large difference in thermal expansion coefficients of Al and Al_2O_3, and the curvature-related pressure gradient across the oxide layer give rise to considerable hoop stresses in the oxide skin which are strongly dependent on the particle size and increase with decreasing particle size of Al.

The RBAO precursor powder consists of a wide particle size distribution. Under the prevailing hoop stresses, the microcracks in the oxide skin of smaller Al particles are extended to macrocracks, while the oxide skin coating larger ones remains stable. In this respect, without *a priori* experimen-

tal determination, a critical size of Al particles was assumed.[8] Calculations assuming a spherical particle yield tensile stresses of 1000 MPa at 500°C in the interface of Al/Al_2O_3 at Al particles <1 μm. Then, in the reaction system, Al oxidation occurs either by oxygen diffusion along the grain boundaries and microcracks in the large particles or, in the smaller particles, by gas diffusion via macrocracks in the oxide skin. Because the latter process is faster than the former, the oxidation of small Al particles dominates in the temperature regime between 450 and 520°C, contributing significantly to the total reaction (e.g. >30%, at T = 520°C). The maximum reaction rate at ~520°C can then be explained: the oxide layer of a certain portion of small Al particles ruptures and complete oxidation takes place. The decomposition of boehmite and diaspore in the surface region of Al particles enhances the rupture process. At >520°C, further reaction occurs only in the remaining Al particles by the aforementioned mechanisms. On the basis of rate control by diffusion through a product layer, the reaction rate is proportional to r^{-2}, where r is the Al particle size.[8] Furthermore, the increased thickness of the oxide layer developed during heating makes the oxygen diffusion path longer. Hence the reaction rate slows down before the metal melts. Consequently, only limited oxidation occurs between 520 and 660°C.

Above the melting temperature (660°C), oxidation of Al is again accelerated. Because of the 8 and 39% volume expansion associated with the melting and oxidation of Al, respectively, the pressure in the interior of Al particles increases until Al permeates into the microcracks, puncturing the scale and spilling into the void space of neighboring particles. Due to bad wetting of Al_2O_3 by liquid Al, droplets form which are readily coated by an oxide skin again. This process continues until all Al is oxidized.

3.3 Kinetics and thermodynamics

The suggested reaction bonding mechanisms are strongly supported by kinetic and thermodynamic studies.[8] Based on isothermal reaction data,[8,12] it has been demonstrated that the reaction kinetics in the RBAO process follow a parabolic rate law in the whole reaction range. The reaction rate depends strongly on the particle size of Al and is controlled by oxygen diffusion.

The activation energy (ΔH) data[8] measured for a pure RBAO system (Al: 45 vol.%, Al_2O_3: 55 vol.%, green density: 64% TD) show very different values in different temperature regimes; i.e. ~112 kJ/mol below the melting temperature of Al and ~26 kJ/mol above the melting temperature. This fact indicates that different reaction mechanisms operate in the respective temperature regimes. Although several mechanisms are involved in the reaction, at a given green density and pore size the oxygen permeability in the RBAO bodies is fixed and the reaction behavior is governed by the reaction system itself;[8] i.e., among parallel alternative mechanisms, the mechanism that requires the lowest activation energy and exhibits the fastest rate dominates the overall oxidation reaction.

In the temperature regime 450–520°C, it is interesting to note that the activation energies for the solid/gas reaction are generally lower than those for oxygen diffusion through lattices in stabilized ZrO_2 (~122 kJ/mol)[13] as well as along grain boundaries in polycrystalline Al_2O_3 (~148 kJ/mol, at T = 1200–1450°C).[14] Without any ZrO_2 additions, the activation energy (~112 kJ/mol) of the sample is still somewhat lower than the quoted value for oxygen lattice diffusion through stabilized ZrO_2. This indicates that lower-energy oxygen transport paths, i.e. diffusion either along the 'porous' grain boundaries or via microcracks through the Al_2O_3 skin, are available.

Above the melting point of Al, the ΔH value is drastically reduced with respect to the solid/gas reaction by a factor of ~5. This is particularly interesting for the understanding of the reaction mechanism in this temperature regime. In the suggested reaction model of the RBAO process described in the previous section, it is assumed that, due to the increased pressure in the interior of Al particles at >660°C, the oxide scale fractures and the molten Al spills into the void space forming droplets. In this situation, the direct contact between oxygen and molten Al would significantly contribute to the overall reaction, reducing the effective activation energy.

4 Modification of the RBAO Process

4.1 ZrO_2-containing RBAO ceramics

In the pure Al/Al_2O_3 RBAO system without ZrO_2 additions, the fracture strength is ~320 MPa at ~93% TD.[8] The microstructure and mechanical properties of RBAO ceramics can be considerably improved by ZrO_2 additions. The grain size decreases with increasing ZrO_2 content as indicated in Fig. 2(a), 2(b) and 2(c) (processing conditions are indicated in the figure caption). The fine distribution of ZrO_2 particles (~0·3 μm) at grain boundaries hinders grain growth in the sintering stage.

RBAO bodies with different porosities can be fabricated by various heat treatments.[15] The bending strengths of RBAO samples fabricated under different conditions and of conventionally sintered

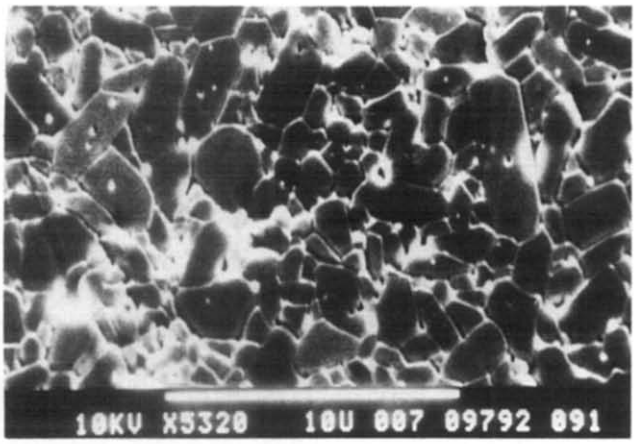

(a)

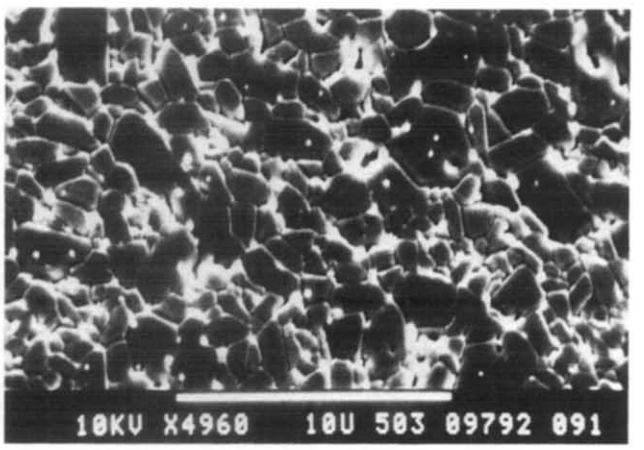

(b)

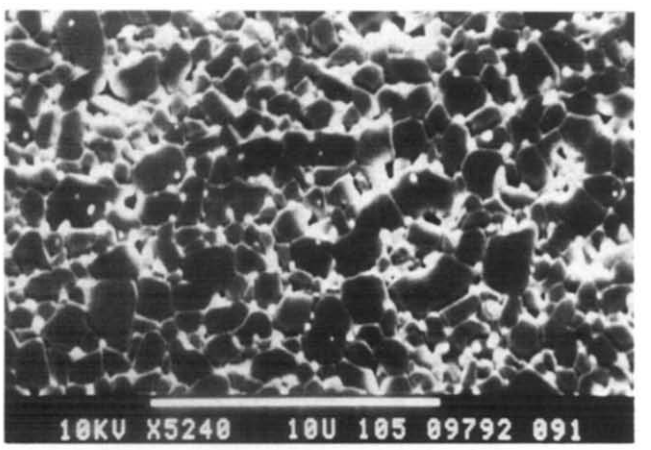

(c)

Fig. 2. Microstructures of ZrO_2-containing RBAO bodies reaction bonded in a one-step cycle (sintering at 1550°C for 2 h). The Al content in all the samples compacted at 300 MPa is 45 vol.%, while that of ZrO_2 in (a) is 2 vol.%, (b) 5 vol.%, and (c) 10 vol.% (the rest is Al_2O_3).

Al_2O_3[16] are given in Fig. 3. The starting RBAO powder mixture consists of 50 vol.% Al, 30 vol.% Al_2O_3 and 20 vol.% ZrO_2. After reaction bonding the final composition is: 82·5 vol.% Al_2O_3 and 17·5 vol.% ZrO_2. To obtain RBAO bodies with various porosities, the precursor powder compacts were heated by different cycles in a box furnace and some of them were then post-HIPed. Sintering and post-HIPing temperatures are indicated in Fig. 3. It is seen from Fig. 3 that at a given porosity the strength of RBAO ceramics is much higher than that of conventional Al_2O_3 and ZrO_2-toughened Al_2O_3. With 20 vol.% ZrO_2 (2Y-TZP) additions, RBAO bodies reaction bonded at up to 1550°C reached final densities of ~97% TD and four-point bending strengths of >700 MPa. After HIPing in Ar at 1500°C and 200 MPa for 20 min, densities and strengths increased to >99% TD and >1100 MPa, respectively (cf. Fig. 3).

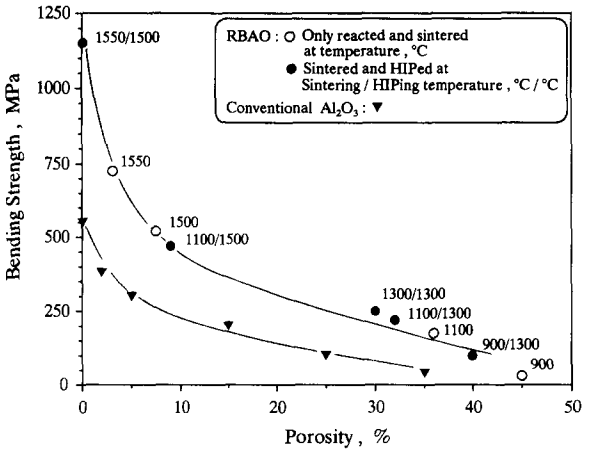

Fig. 3. Bending strengths of RBAO[15] and conventional Al_2O_3 ceramics.[16]

In recent years, porous Al_2O_3 has been of great interest for many industrial applications, such as catalytic converter filters, electrolytic membranes and gas distributors.[17] In this respect, the RBAO technique together with post-HIPing would provide a promising fabrication route for high-strength porous ceramics.

4.2 Nb_2O_5-containing RBAO ceramics

An RBAO precursor powder consisting of Al (40 vol.%), orthorhombic Nb_2O_5-stabilized ZrO_2 (Nb-OZP, 20 vol. %), Al_2O_3 (30 vol.%) and Nb (10 vol. %) powders was processed by the standard RBAO route.[18] In spite of the high compaction pressure of 900 MPa used, Al and Nb oxidize

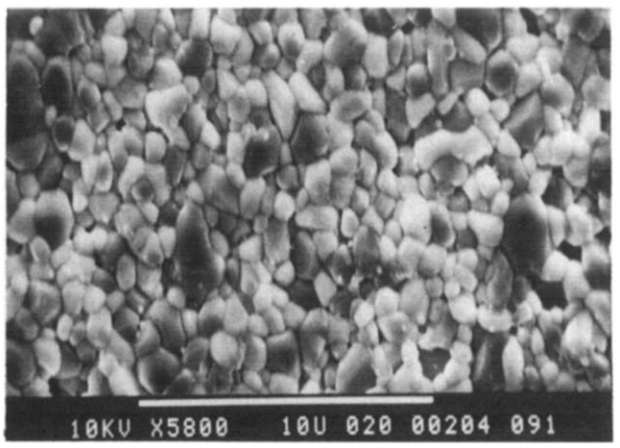

Fig. 4. Microstructure of Nb-containing RBAO sintered at 1400°C for 1 min.[18]

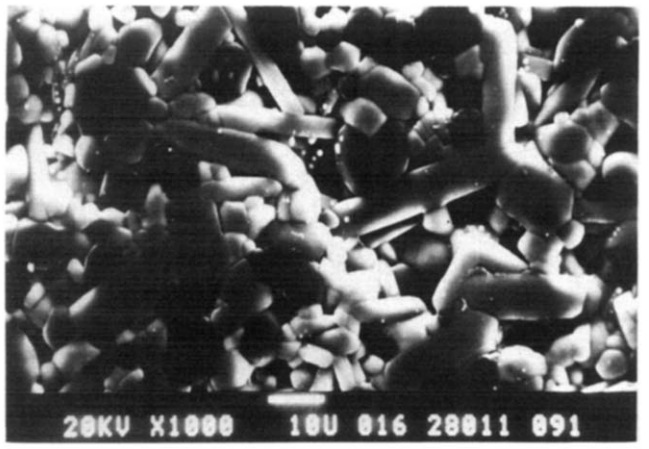

Fig. 5. Microstructure of Nb-containing RBAO showing needle-like grains formed *in situ* after aging at 1400°C for 24 h.[18]

completely at temperatures <900°C. Nb additions assist in reducing the sintering shrinkage by a large volume expansion on oxidation. After sintering at 1400°C for 1 min, a shrinkage of ~3·5% at a final density of 90% TD was obtained. Equiaxed small (<1 μm) and relatively large (~3 μm) grains coexist in the microstructure as shown in Fig. 4. The small particles are formed during the reaction process, whereas the large ones are the originally admixed Al_2O_3 particles. Fracture strength and toughness of the sample are ~330 MPa and ~3 MPa·m$^{1/2}$, respectively.

An interesting feature of this material is the in-situ formation of needle-like grains with high aspect ratio as shown in Fig. 5, which occurs during aging of the specimen at 1400°C for 24 h. The needle-like grains consist predominantly of complex oxide compounds of Zr and Nb, with Al as minor phase, whereas the matrix grains, in addition to Al_2O_3, consist of either Nb_2O_5 and ZrO_2 or Nb_2O_5 and Al_2O_3 reaction products. This in-situ formation of enlongated grains was only observed when Nb-OZP is present. It has been found that Ca also triggers rapid in-situ growth of elongated grains.[18] Samples which have been pressurelessly. infiltrated with aqueous $Ca(NO_3)_2$ solution prior

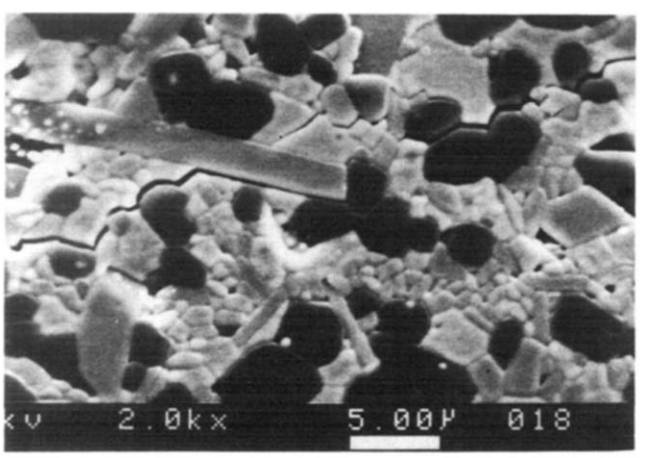

Fig. 6. Crack deflection and crack wave interaction in Nb_2O_5/ZrO_2-RBAO.[18]

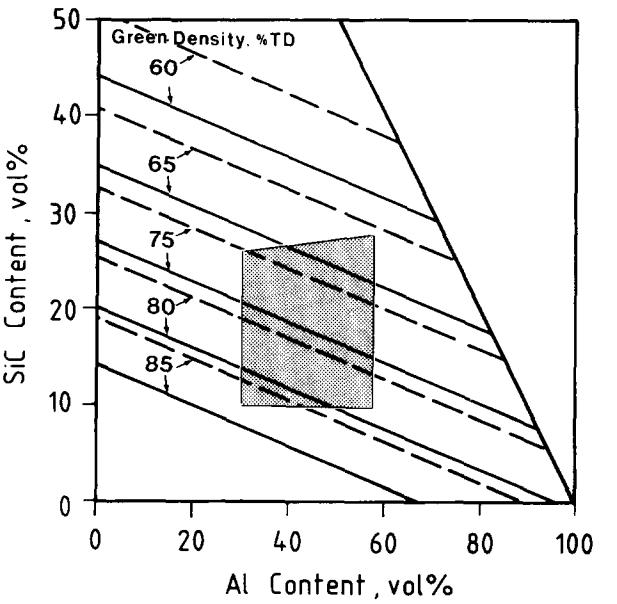

Fig. 7. Theoretical conditions (according to eqn (1)) for zero shrinkage at (——) 95 and (– – –) 100% TD. Required green densities (% TD) are indicated. The area in the upper right of the diagram has no physical meaning since the compositional sum exceeds 100%.[7]

to the sintering step showed grain aspect ratios of >6 even after only 1 min at 1400°C. However, longer aging times do not significantly alter either the aspect ratio or the amount of needle-like grains. The dispersion of matrix particles hinders grain growth and separates the needle-like grains. Consequently, the microstructure becomes relatively stable when the elongated grains begin to contact each other. These needle-like grains act as reinforcement particles by mechanisms such as crack deflection and crack bridging (cf. Fig. 6). Fracture toughness can then be improved, e.g. 5·3 MPa·m$^{1/2}$ was achieved for the $Ca(NO_3)_2$-infil-

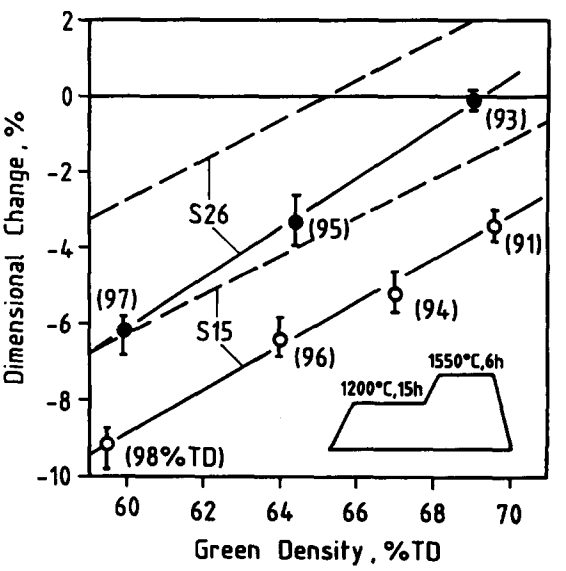

Fig. 8. Dimensional changes of reaction-bonded mullite composites S15 (Al, 40; Al_2O_3, 45; SiC, 15 vol.%) and S26 (Al, 40; Al_2O_3, 34; SiC, 26 vol. %) as function of green density. Final relative densities are given in brackets, with theoretical final density of (——) 95 and (– – –) 100% TD.[7]

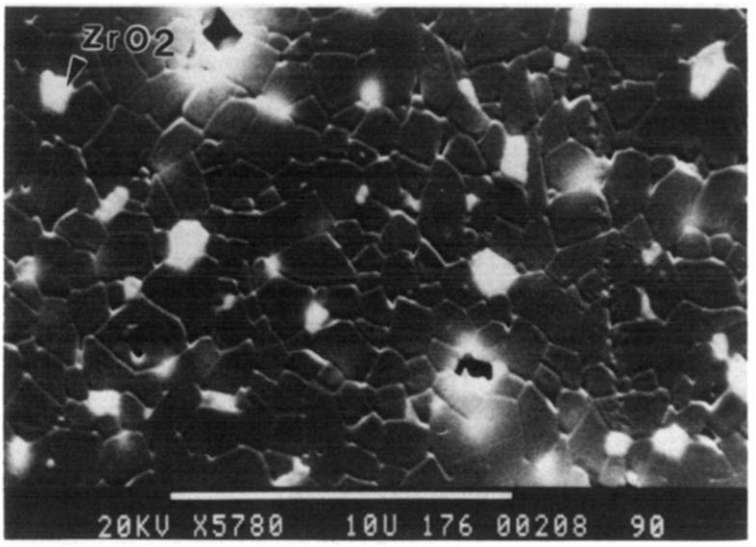

Fig. 9. Microstructure of a sample (S26; see figure caption of Fig. 8) isopressed at 160 MPa and heated through the complete cycle indicated in Fig. 8.[7]

trated sample. This approach may provide a promising route for in-situ whisker reinforcement of ceramics without the usual problems such as mixing inhomogeneity and health hazard.

4.3 Reaction-bonded mullite composites

Based on the RBAO technology, low-to-zero shrinkage mullite and mullite composites have been fabricated starting from $Al/Al_2O_3/SiC$ powder mixtures.[7] Because of the volume expansion associated with the oxidation of Al (28%) and SiC (108%) and with mullite formation (4·2%), sintering shrinkage is effectively compensated. According to eqn (1), conditions for zero shrinkage at final density of 95 and 100% TD are indicated in Fig. 7, with fractional green densities as parameters and the assumption that during milling Al is not oxidized; i.e. $f = 0$, and that Al and SiC additions are fully oxidized. These conditions indicate that net-shape forming in this system is possible. In practice, however, the Al content should not exceed 60 vol.% for safe handling of the RBAO process, and the SiC content should be chosen by considering the desired phase composition in the final product. If the purpose is to make pure mullite or mullite/Al_2O_3 composites, compositions in the trapezoid region shaded in the center of the diagram in Fig. 7 would be advisable. The compositions along the top boundary result in pure mullite, while other compositions in the region result in mullite/Al_2O_3 composites.

To oxidize the SiC particles fully, the heating cycle should usually consist of two steps: reaction (<1200°C) and sintering (1400–1550°C). Experimental data showing dimensional changes of two samples as a function of green density are given in Fig. 8. Sample compositions and experimental conditions are indicated in the figure caption. Unlike sintering of normal ceramic powder compacts, the final density decreases with increasing green density (cf. Fig. 8). This is probably due to some unoxidized SiC remaining until the end of the oxidation step. With increasing temperature, the local pore system closes more rapidly in samples with higher green densities. Hence CO/CO_2 gas is trapped and, because of the insolubility of the CO_2 molecules, pore removal becomes increasingly difficult. This indicates that in the fabrication of pure mullite or mullite/Al_2O_3 composites the heating cycle should be carefully controlled such that SiC particles are fully oxidized before sintering. In this respect, ultrafine SiC powders and lower oxidation temperatures are of advantage.

The microstructure of a reaction-bonded mullite sample is shown in Fig. 9. The fracture strengths of fully reaction-bonded mullite composites consisting of 60 vol.% mullite/37 vol.% Al_2O_3/3 vol.% ZrO_2 and 97 vol.% mullite/3 vol.% ZrO_2 are 380 and 290 MPa at 98 and 97% TD, respectively. The ZrO_2 phase in the final products originates from the wear debris of TZP milling balls.

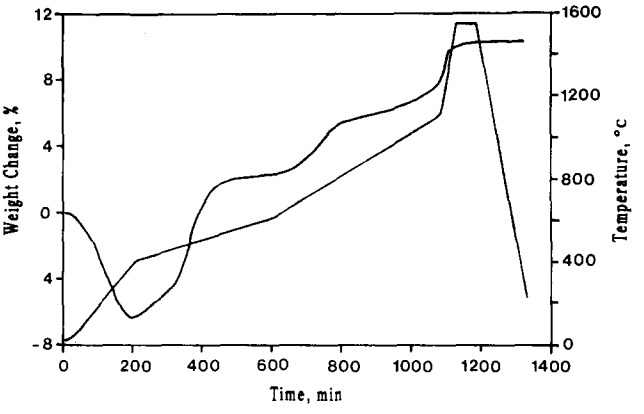

Fig. 10. Weight change of a sample (Al, 40; Al_2O_3, 30; SiC, 30 vol.%) compacted at 300 MPa during heat treatment.

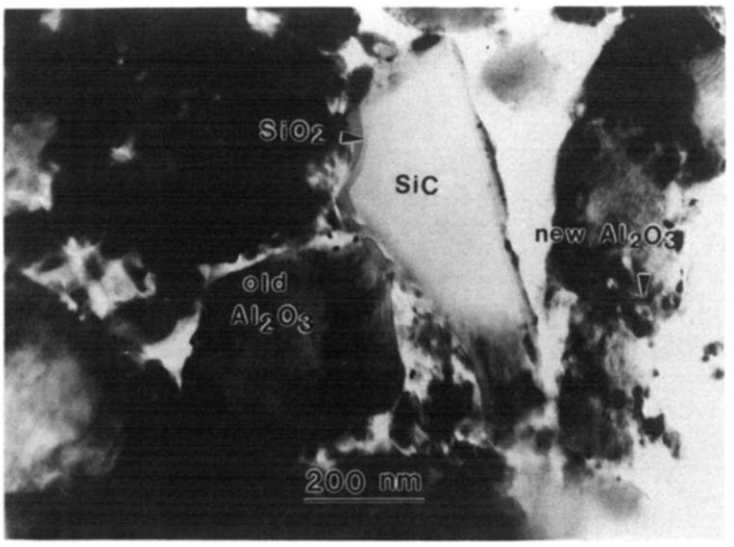

Fig. 11. TEM micrograph of the same sample as in Fig. 10 heated to 1100°C in air without hold at the temperature.

If the starting SiC powder and heating cycle are selected such that the SiC particles are not completely oxidized, various mullite composites can be obtained, e.g. mullite/SiC, mullite/Al_2O_3/SiC, etc. A powder mixture of 40 vol.% Al, 30 vol.% Al_2O_3 and 30 vol.% SiC was attrition milled with ZrO_2 balls for 7 h. Because of the aggressiveness of the coarse SiC (~6 μm) used, a substantial amount of ZrO_2 wear debris (~20%) was introduced into the mixture. Figure 10 shows the weight change of such a powder compact isopressed at 300 MPa as a function of a heating cycle which does not contain an oxidation hold for SiC. The reaction behavior of Al is similar to that observed in the pure RBAO system.[6,8,9] Due to the slow heating rate (<1°C/min), Al oxidizes completely at <820°C. It is difficult to determine the exact temperature at which SiC oxidation begins; however, further weight increase at >820°C would be a clear indication for this reaction. Up to 1100°C, SiC particles oxidize to SiO_2 only on their surface, as shown in the TEM micrograph in Fig. 11. Above 1100°C, the heating rate was increased to 10°C/min to avoid much further oxidation. Reaction between Al_2O_3 and SiO_2 to give mullite occurs at ~1400°C.[7] The mullite formation prevents further oxidation of the SiC particles, therefore the sample exhibits no significant weight increase at temperatures >1400°C. The final microstructure of the sample is shown in the TEM micrograph in Fig. 12. The phase composition after reaction bonding is ~55 vol.% mullite, 10 vol.% SiC, 21 vol.% Al_2O_3 and 14 vol.% ZrO_2. The grain size of the microstructure is well below 1 μm. SiC particles are found both in mullite grains and at grain boundaries, while most ZrO_2 particles with irregular shapes are distributed at grain boundaries. TEM investigation shows that almost all ZrO_2 in the

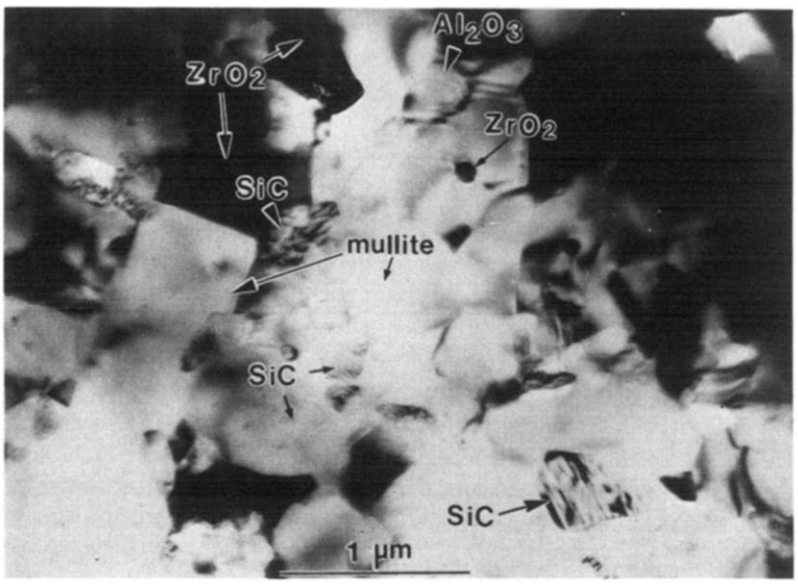

Fig. 12. TEM micrograph of the same sample as in Fig. 10 after completion of the heating cycle presented in Fig. 10. The final product consists of ~55 vol.% mullite, 10 vol.% SiC, 21 vol.% Al_2O_3 and 14 vol.% ZrO_2. The ZrO_2 originated from the wear debris of TZP milling balls.

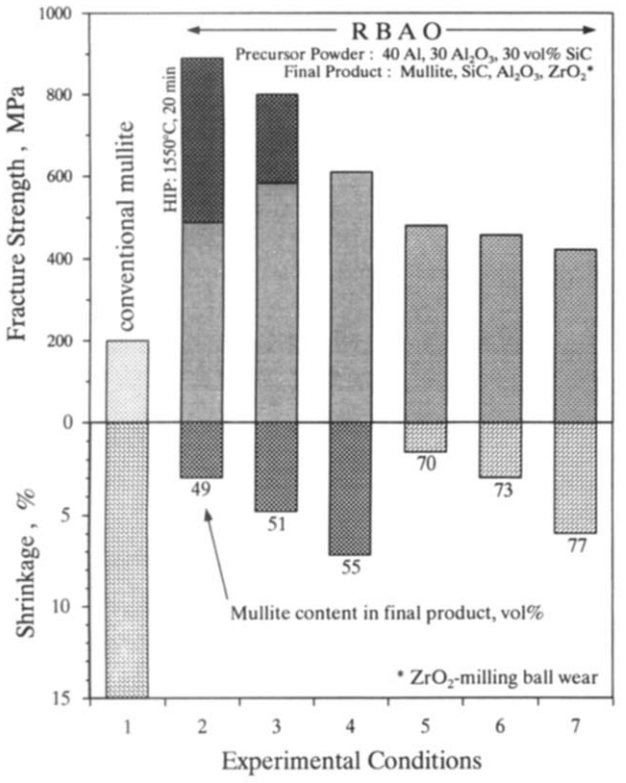

Experimental Conditions		
	Compaction Pressure MPa	Heat-Treatment Cycle
1		1650°C
2	900	1550°C, 1h; 10°C/min; 1100°C; 10°C/min; 1°C/min
3	600	
4	300	
5	900	1550°C, 1h; 10°C/min; 1150°C, 5h; 10°C/min; 1°C/min
6	600	
7	300	

Fig. 13. Fracture strengths, shrinkages and experimental conditions of conventional mullite ceramics and RBAO-type mullite/SiC composites.

ion-beam-thinned sample is in monoclinic morphology, whereas XRD analysis on carefully polished surfaces of the same sample indicate that most of ZrO_2 is tetragonal. The XRD intensity ratio of monoclinic/tetragonal phase in the fractured surface is ~28% higher than that in the polished surface. These are clear indications for the t- to m-ZrO_2 phase transformation taking place during either ion-beam-thinning or fracturing.

By changing the heat-treatment cycle, various phase ratios of mullite/SiC result in the final products. In spite of high final densities (>96% TD), the reaction-bonded bodies exhibit low linear shrinkages and superior mechanical properties. For example, shrinkages of 7·2, 4·8 and 3%, and strengths of 610, 583 and 489 MPa, corresponding to a compaction pressure of 300, 600 and 900 MPa, respectively, were achieved in samples containing 49–55 vol.% mullite. Fracture strengths, shrinkages and experimental conditions of such mullite/SiC composites and those of conventional mullite ceramics are given in Fig. 13. HIPing can significantly improve the mechanical properties of the reaction bonded mullite/SiC composites, as indicated in Fig. 13. For example, after HIPing at 1550°C and 200 MPa in Ar for 20 min, the strength and toughness of the sample containing 49 vol.% mullite increase from 490 to 890 MPa and from 4 to 5·9 MPa·$m^{1/2}$, respectively. These unusually high strengths of the reaction-bonded mullite/SiC/ZrO_2 composites are attributed to the small grain size and transformation toughening of ZrO_2.

These low-shrinking mullite compositions should represent ideal matrices for high-strength high-density composites, e.g. with sapphire or SiC fibers.

4.4 Platelet- and fiber-reinforced RBAO composites

In the pure RBAO system, shrinkages can be controlled exactly to zero at the expense of final densities. In this respect, the sintering temperature is usually <1300°C and the reaction-bonded bodies contain 20–35% porosity. Such bodies can also be used for the incorporation of coarse second phases, such as platelets and fibers. The remaining pores can be filled by metal infiltration such as to obtain metal/ceramic composites. In this approach, two examples are now given.

In a study of fiber-reinforced RBAO ceramics,[19] 30 vol.% of a ZrO_2-toughened Al_2O_3 fiber (~50–

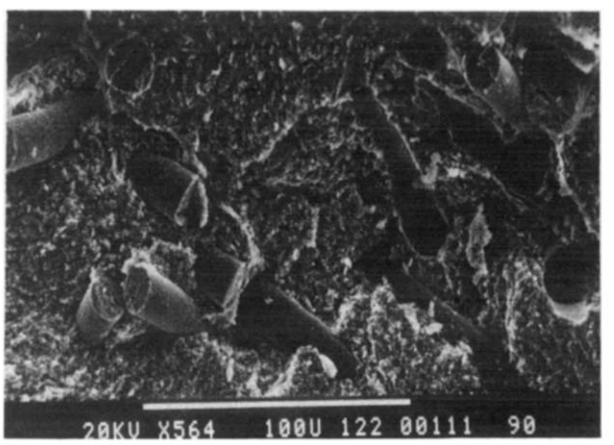

Fig. 14. Fracture surface of a fiber-reinforced RBAO body compacted at 300 MPa and reaction bonded at 1250°C for 5 h.

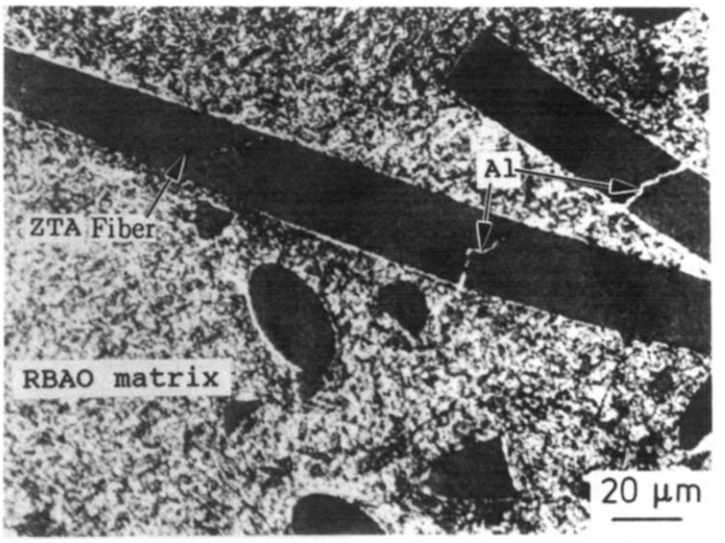

Fig. 15. Polished surface of an Al-infiltrated RBAO/fiber composite.

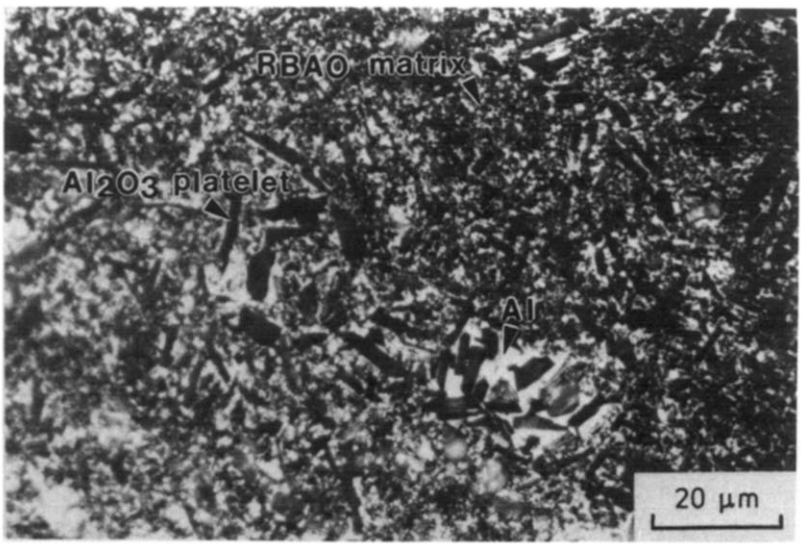

Fig. 16. Polished section of an Al-infiltrated RBAO/platelet composite.

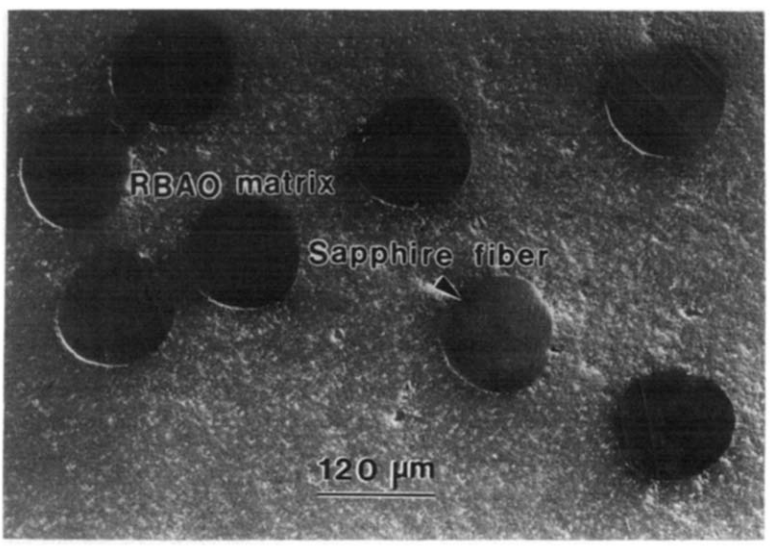

Fig. 17. Polished section of an RBAO/sapphire fiber (continuous) composite.

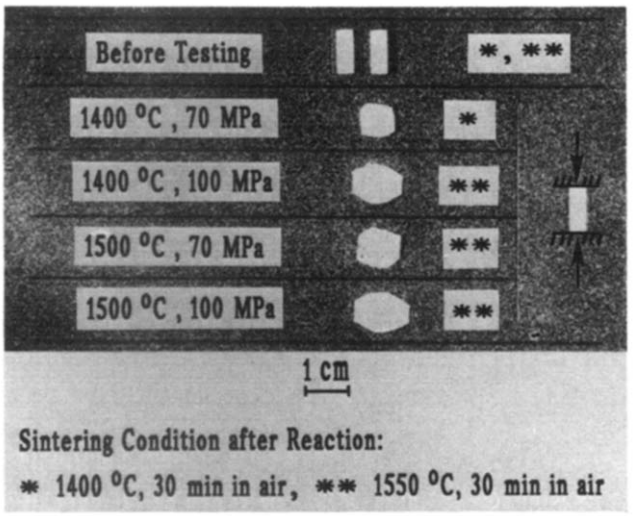

Fig. 18. Superplastic tests on RBAO samples which were sintered at (*) 1400°C and (**) 1550°C for 30 min. Test conditions are indicated on the left-hand side of the samples.

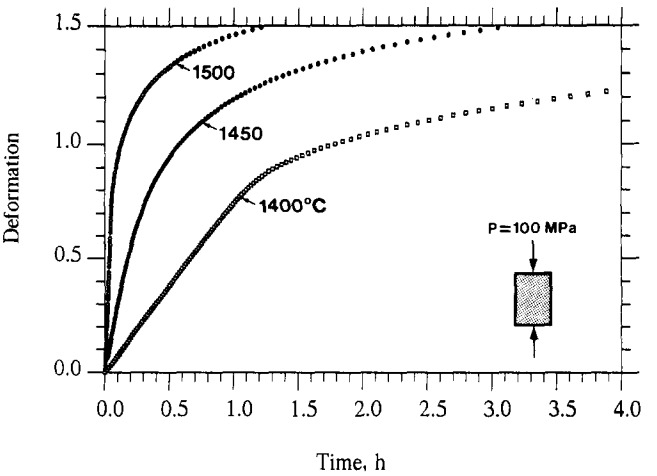

Fig. 19. Superplastic deformation of RBAO samples sintered at 1550°C for 2 h as a function of time and temperature at a constant pressure of 100 MPa.

250 μm long, ~20 μm diameter) was randomly admixed into an RBAO precursor powder consisting of 50 vol.% Al, 30 vol.% Al_2O_3, and 20 vol.% ZrO_2. The mixture was isopressed at 300 MPa and reaction bonded at 1250°C for 5 h. The body exhibited zero shrinkage at final density of ~71% TD. Figure 14 shows a fracture surface of the sample in which pull-out of the fibers is clearly visible. In spite of high porosity, the fracture strength and toughness of the sample are 80 MPa and 2·1 MPa·$m^{1/2}$, respectively. After Al infiltration, the strength and toughness increased to 580 MPa and 5·8 PMa·$m^{1/2}$, respectively. The micro-structure of the infiltrated sample is shown in Fig. 15. Cracks and gaps in and around the fibers generated during processing were filled with Al, hence they no longer fully act as strength-controlling flaws.

Al_2O_3 platelets (30 vol.%; ~13 μm) were incorporated in an RBAO precursor powder consisting of 40 vol.% Al and 60 vol.% Al_2O_3.[20] Compacts isopressed at 400 MPa and heat treated at 1200°C for 15 h exhibited no dimensional change at a final density of ~76% TD. After Al infiltration, fracture strength of the composite increased from 85 to 760 MPa, and toughness from 1·6 to 5·8 MPa·$m^{1/2}$, respectively. The microstructure of the infiltrated sample is shown in Fig. 16. Due to short mixing periods, the powder compact contained localized platelet agglomerates. After infiltration, Al filled the void space both in the RBAO matrix and the agglomerates.

An important potential of the RBAO ceramics is to incorporate continuous fibers (e.g. sapphire fibers). Initial investigations show promising results. Figure 17 shows a polished section of an RBAO/sapphire fiber (continuous) composite. In spite of the large diameter (~120 μm), the fibers are well accommodated in the as-bonded RBAO matrix without crack formation.

4.5 Superplasticity

Numerous experimental phenomena show that RBAO bodies exhibit superplastic behavior, e.g. bloating during heat treatment[9] when the sample contains chemically bonded water which has not been removed up to ~1200°C. Initial explorations have confirmed this superplasticity in RBAO ceramics. A precursor powder consisting of 35 vol.% Al, 45 vol.% Al_2O_3 and 20 vol.% ZrO_2 was reaction bonded up to 1400°C and 1550°C for 30 min, resulting in final densities of ~90 and 95% TD, respectively. Final phase composition was 82 vol.% Al_2O_3 and 18 vol.% ZrO_2. The samples were cut into rectangular parallelepipeds of 4 mm × 4 mm × 10 mm. Testing was performed in air at different temperatures under compression (70 and 100 MPa) normal to the square sections. All samples were deformed to thin sheets (<1 mm) without cracking, as shown in Fig. 18. Deformation data of a sample of the same composition sintered at 1550°C for 2 h (final density: 97% TD) as a function of time at a constant pressure of 100 MPa are given in Fig. 19. It would be expected that the superplasticity of the RBAO bodies can be enhanced at higher Al (>40 vol.%) and ZrO_2 (>20 vol.%) contents in the starting powder mixtures, since these favor a fine microstructure in the reaction bonded bodies.

5 Conclusions

(1) The RBAO process proceeds both by solid/gas and liquid/gas reactions, independent of additives, i.e. also without ZrO_2 additions. Below the melting temperature of Al, oxygen diffusion through the oxide skin of Al dominates, while above the melting temperature, Al droplets spilling out of molten Al pool are responsible for the reaction.

(2) The reaction rate is controlled by oxygen diffusion and follows a parabolic relationship. In a given system, it depends strongly on Al particle size.
(3) The measured activation energy data render strong support to the reaction mechanisms suggested for the RBAO process.
(4) Process, product, and reaction mechanisms are completely different from those of directed molten metal oxidized composites; i.e. DMO (Lanxide^{TM})[1] composites.
(5) The RBAO process can be modified by incorporation of other ceramic or metal additives either to improve microstructure or to reduce shrinkage.
(6) ZrO_2 additions have a very positive effect on the microstructural evolution, promoting a finer and more homogeneous microstructure in the fully reaction-bonded bodies. High densities can be achieved in ZrO_2-containing RBAO ceramics. Due to homogeneous microstructure and small grain size, ZrO_2-containing RBAO ceramics exhibit high strengths, e.g. >700 MPa at 97% TD and >1100 MPa at >99% TD after HIPing.
(7) The RBAO technique together with post-HIPing provides a promising fabrication route for high strength porous ceramics.
(8) In the presence of orthorhombic Nb_2O_5-stabilized ZrO_2 (Nb-OZP), Nb-containing RBAO precursor powders result in in-situ formation of needle-like grains which act as reinforcements and thus improve fracture toughness of the resulting composites.
(9) Net-shape forming is possible in the system $Al/Al_2O_3/SiC$. Mullite/SiC composites with low-shrinkages at high densities can be obtained by changing heating cycles. These materials exhibit also fine microstructures and high mechanical properties, e.g. strengths of ~490–610 MPa for composites consisting of 49–55 vol.% mullite. HIPing significantly improves the mechanical properties. For example, after HIPing, fracture strength and toughness increase from ~490 MPa and ~4 MPa·m$^{1/2}$ at ~96% TD to ~890 MPa and 5·9 MPa·m$^{1/2}$ at >99% TD, respectively. These low-shrinking mullite compositions should represent ideal matrices for high-strength high-density composites, e.g. with sapphire or SiC fibers.
(10) Considerable improvement in mechanical properties can be achieved in porous RBAO bodies consisting of second-phase particles by metal infiltration. For example, strength and toughness increase from 85 to 760 MPa and 1·6 to 5·8 MPa·m$^{1/2}$, respectively, for platelet-reinforced RBAO after Al infiltration.
(11) The RBAO ceramics exhibit superplastic transformability.
(12) The versatility and further aspects of RBAO technology are indicated by the 'Japanese Tree' in Fig. 20.

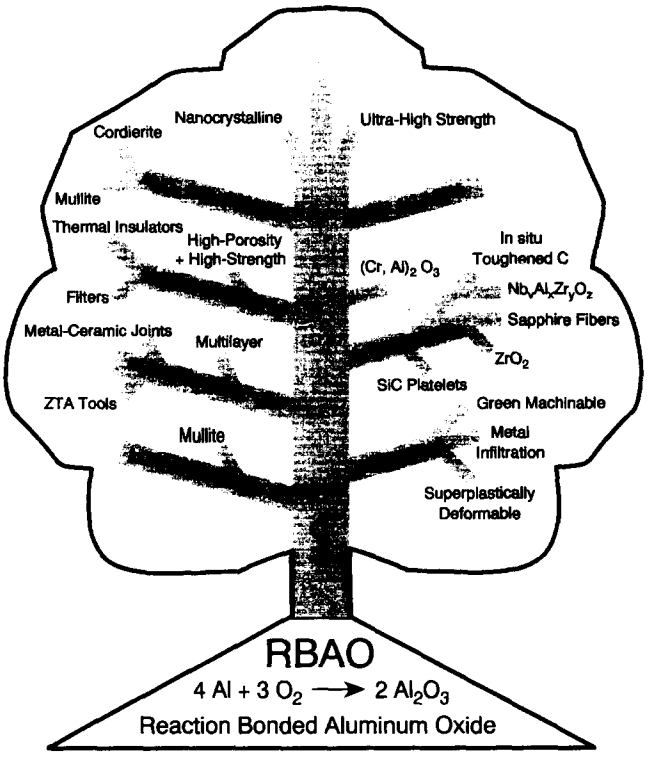

Fig. 20. 'Japanese tree' showing the various directions RBAO technology has taken.

Acknowledgements

The authors thank the Deutsche Forschungsgemeinschaft (DFG) for financial support under contracts No. Cl 52/10 and No. Cl 52/12-2. Thanks are also due to D. Garcia for his contribution on Nb-containing RBAO.

References

1. Newkirk, M. S., Urquhart, A. W., Zwicker, H. R. & Breval, E., Formation of Lanxide^{TM} ceramic composite materials. *J. Mater. Res.*, **1** (1986) 81–9.
2. Claussen, N. & Urquhart, A. W., Directed oxidation of molten metals. In *Encyclopedia of Mat. and Eng.*, Supplementary Vol. 2, ed. R. W. Cahn. Pergamon, Oxford, 1990, pp. 1111–15.
3. Sindel, M., Travitzky, N. A. & Claussen, N., Influence of Mg–Al-spinel on the directed oxidation of molten aluminum alloys. *J. Am. Ceram. Soc.*, **73** (1990) 2651.
4. Anatolin, S., Nagelberg, A. S. & Creber, D. K., Formation of Al_2O_3/metal composites by the directed oxidation of molten Al–Mg–Si alloys. *J. Am. Ceram. Soc.*, **75** (1992) 447.
5. Claussen, N., Le, T. & Wu, S., Low-shrinkage reaction-bonded alumina. *J. Eur. Ceram. Soc.*, **5** (1989) 29–35.

6. Claussen, N., Travitzky, N. A. & Wu, S., Tailoring of reaction-bonded Al_2O_3 (RBAO) ceramics. *Ceram. Eng. Sci. Proc.*, **11** (1990) 806–20.
7. Wu, S. & Claussen, N., Fabrication and properties of low-shrinkage reaction-bonded mullite. *J. Am. Ceram. Soc.*, **74** (1991) 2460–3.
8. Wu, S., Holz, D. & Claussen, N., Mechanisms and kinetics of reaction-bonding Al_2O_3 (RBAO) ceramics. *J. Am. Ceram. Soc.*, **76** (1993) 970–80.
9. Holz, D., Wu, S., Scheppokat, S. & Claussen, N., Effect of processing parameters on phase and microstructure evolution in RBAO ceramics. *J. Am. Ceram. Soc.*, **77** (1994) (in press).
10. Xue, L. A. & Chen, I. W., Influence of additives on γ-to-α transformation of alumina. *J. Mater. Sci. Lett.*, **11** (1992) 443–5.
11. Beck, A. F., Heine, M. A., Caule, E. J. & Pryor, M., The kinetics of the oxidation of Al in oxygen at high temperature. *Corros. Sci.*, **7** (1967) 1–22.
12. (a) Carter, R. E., Kinetic model for solid-state reactions. *J. Chem. Phys.*, **34** (1960) 2010–16. (b) Carter, R. E., Kinetic model for solid-state reactions. *J. Chem. Phys.*, **35** (1961) 1137–8.
13. Howard, R. E. & Lidiard, A. B., Matter transport in solids. *Rep. Pro. Phys.*, **27** (1964) 161–240.
14. Kingery, W. D., Bowen, H. K. & Uhlmann, D. R., *Introduction to ceramics*. 2nd ed. John Wiley & Sons, NY, 1976.
15. Holz, D., Geerken, M., Wu, S., Janssen, R. & Claussen, N., HIP of reaction-bonded alumina (RBAO) with various ratios of open-to-closed porosity. In *Proceedings of HIP '93, 21–23 April 1993, Antwerp, Belgium, ed. L. Delaey, H. Tas & W. Kaysser. Elsevier*, pp. 425–33.
16. Knechtel, M., PhD thesis, Technische Universität Hamburg–Harburg, Hamburg, Germany, 1995 (to be published).
17. Ishizaki, K., Takata, A. & Okada, S., Mechanically enhanced open porous materials by HIP process. *J. Ceram. Soc. Japan.*, **98** (1990) 545–51.
18. Garcia, D. E., Janssen, R. & Claussen, N., In-situ reinforced reaction bonded aluminum oxide (RBAO). In *Third Euro-Ceramics*, Vol. 3, *Engineering Ceramics*, ed. P. Duran & J. F. Fernandez. Faenza Editrice Iberica, S.L., 1993, pp. 719–24.
19. Wu, S. & Claussen, N., Net-shape forming of RBAO-composites. Presented at The 3rd IUMRS International Conference on Advanced Materials, Tokyo, Japan, 31 August–4 September 1993.
20. Wu, S., Gesing, A., Travitzky, N. A. & Claussen, N., Fabrication and properties of Al-infiltrated RBAO-based composites. *J. Eur. Ceram. Soc.*, **7** (1991) 277–81.